

Surface-State Bands on Silicon —Si(111)- $\sqrt{3} \times \sqrt{3}$ -Ag Surface Superstructure—

Shuji HASEGAWA^{1,2}, Norio SATO¹, Ichiro SHIRAKI¹, Cristian L. PETERSEN³, Peter BØGGILD³,
Torben M. HANSEN³, Tadaaki NAGAO^{1,2} and François GREY³

¹Department of Physics, University of Tokyo, Hongo 7-3-1, Bunkyo-ku, Tokyo 113-0033, Japan

²Core Research for Evolutional Science and Technology, Japan Science and Technology Corporation,
4-1-8 Honcho, Kawaguchi, Saitama 332-0012, Japan

³Mikroelektronik Centret, Technical University of Denmark, Bldg. 345 east, DK-2800 Lyngby, Denmark

(Received February 9, 2000; accepted for publication March 16, 2000)

After reviewing the atomic and electronic structures of the Si(111)- $\sqrt{3} \times \sqrt{3}$ -Ag surface, which have recently been clarified after much research, we describe the experimental confirmations of electrical conduction through its surface-state band. A newborn method, micro-four-point probe, is introduced for conductivity measurements with high surface sensitivity.

KEYWORDS: silicon surface, surface electronic state, surface superstructure, scanning tunneling microscopy, surface electrical conduction, four-point probe

1. Introduction

The Si(111)- $\sqrt{3} \times \sqrt{3}$ -Ag surface superstructure, which is formed by depositing one monolayer (ML) of Ag atoms on a Si(111) surface at temperatures higher than 250°C, has been a long-standing target in surface science because of the interesting physics revealed in its atomic arrangement, surface electronic states, and electronic transport phenomena.¹⁾ After much controversy spanning over a period of 20 years, its atomic arrangement was solved by the so-called “Honeycomb-Chained Triangle (HCT)” model.^{2–5)} This surface is now regarded as a prototypical metal-covered semiconductor system, and is used as a standard sample for *e.g.*, high-resolution photoemission spectroscopy (PES),⁶⁾ atomic force microscopy,^{7–9)} X-ray diffraction for buried interface structure analysis,^{10–12)} Schottky barrier formation^{13–15)} optical second-harmonics generation spectroscopy,¹⁶⁾ first-principles theory,^{17–19)} as well as a unique substrate for the growth of C₆₀ molecular layers,^{20–23)} adatom gas phase,²⁴⁾ and other surface superstructures by additional metal and hydrogen adsorptions.^{25–33)} However, it was recently revealed that the HCT structure is not a ground-state structure; a

symmetry-broken phase, the so-called “InEquivalent Triangle (IET)” structure, is more energetically favorable than the HCT structure.^{34,35)}

This superstructure has a characteristic surface electronic state; an isotropic and parabolic surface-state band crossing the Fermi level (E_F) was revealed by angle-resolved PES,^{36–40)} indicating a two-dimensional free-electron-like system. Thus this surface provides a unique platform for low-dimensional physics such as electronic transport because its “thickness” is as small as one or two atomic layers, which is much thinner than conventional two-dimensional electron gas (2DEG) systems formed at surface inversion layers or heterojunctions. Though new quantum phenomena in electronic transport through the surface-state band are not yet known, we will show here direct measurements of the surface-state electrical conduction on this surface, together with a review of its atomic and electronic structures.

2. Atomic Structure

2.1 Ground-state structure

Figure 1 displays a series of scanning electron micrographs (SEM) of a mesoscopic region on a Si(111) surface in ul-

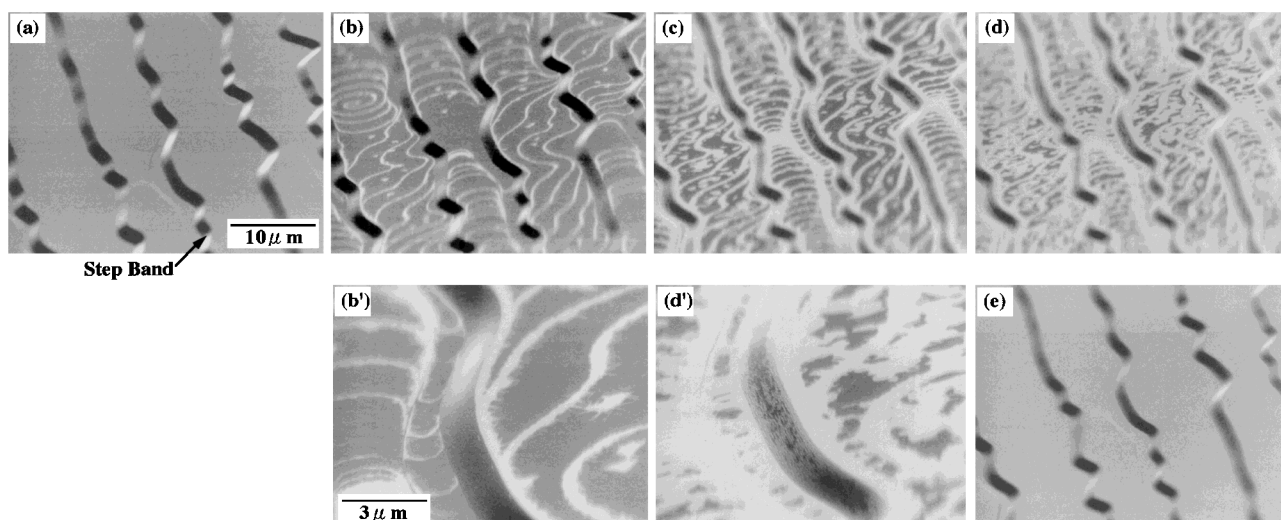


Fig. 1. Grazing-incidence ultrahigh-vacuum scanning electron micrographs, showing a conversion from the 7×7 clean surface (a) into the $\sqrt{3} \times \sqrt{3}$ -Ag (e) during Ag deposition at 450°C. The glancing angle of the primary electron beam was about 10°, so that the images were foreshortened by a factor of about 5 in the vertical direction. (b') and (d') are magnified images of (b) and (d), respectively.

trahigh vacuum (UHV), showing a structural transformation from a clean 7×7 surface (a) to the $\sqrt{3} \times \sqrt{3}$ -Ag superstructure (e) by depositing Ag at a substrate temperature of 450°C . The surface was composed of flat terraces about $10 \mu\text{m}$ wide and step bands about $2 \mu\text{m}$ wide, with around 50 atomic steps accumulated. The adsorbed Ag atoms initially nucleate at monatomic step edges on the flat terraces (see Fig. 1(b)), where the atomic arrangement converts into the $\sqrt{3} \times \sqrt{3}$ -Ag domains. The brighter areas are the $\sqrt{3} \times \sqrt{3}$ -Ag domains, and the darker ones, the 7×7 clean domains. With an increase in Ag coverage, the brighter areas grow, and the entire surface is finally covered by the $\sqrt{3} \times \sqrt{3}$ -Ag superstructure by 1 ML Ag adsorption (see Fig. 1(e)). Thus, the emission yield of secondary electrons is considerably different depending on the surface superstructures of the topmost layers, due to a change in the surface electronic states.⁴¹⁾

Figure 2(a) illustrates the HCT model, which is believed to be the most stable atomic arrangement for the $\sqrt{3} \times \sqrt{3}$ -Ag superstructure (at least) at room temperature (RT).²⁻⁵⁾ The topmost Si atoms (large open circles) make trimers, each of which forms an ionic covalent bond with a Ag atom (filled circles) to make Ag triangles. This model well explains its scanning tunneling micrographs (STM)^{17,18)} of (b) the empty state and (c) the filled state at RT. Protrusions in the empty-state image, corresponding to the centers of Ag triangles, are arranged in a honeycomb-lattice pattern in Fig. 2(b). However, at lower temperature (62 K), its empty-state image (Fig. 2(e)) shows a different feature, a hexagonal-lattice pattern, instead of the honeycomb one.⁴²⁾ This turns out to correspond to a new model for the surface, the IET model, in which Ag tri-

angles, all of which are equivalent in the HCT model, differ in size alternately. As shown in the schematic of the atomic arrangement (Fig. 2(d)) for the IET model, a Ag triangle in a half-unit cell becomes larger (called L-half) and another triangle in the other half-unit cell becomes smaller (S-half). In other words, a mirror plane along the $[1\bar{2}1]$ direction in the HCT model (belonging to $p31m$ space group) disappears in the IET model (belonging to $p3$ space group), a kind of *symmetry breakdown*. The protrusions in the low-temperature STM image (Fig. 2(e)) correspond to the S-half unit cell. A first-principles calculation showed that the IET structure is more stable than the HCT by 0.1 eV per $\sqrt{3} \times \sqrt{3}$ unit cell.³⁴⁾

Then, we are faced with new, interesting questions about this surface: what is the relationship between the HCT and IET structures? There should be a phase transition between them by temperature change. What is the nature of the phase transition? Moreover, it is not certain whether the HCT structure can be understood as a time-averaged structure of a fluctuating IET structure, much like symmetric dimers on a clean Si(001) surface at RT which are time-averaged buckled dimers. This surface is still a challenging target in surface physics.

2.2 Domain boundaries

The $\sqrt{3} \times \sqrt{3}$ -Ag superstructure in the HCT phase has conventional out-of-phase domain boundaries (OPBs), as shown in Figs. 3(a) and 3(b), due to a phase mismatch in the super-periodicity between adjacent domains.⁴³⁾ However, when cooled to lower temperatures to transform the surface into the IET phase, the surface splits into two types of do-

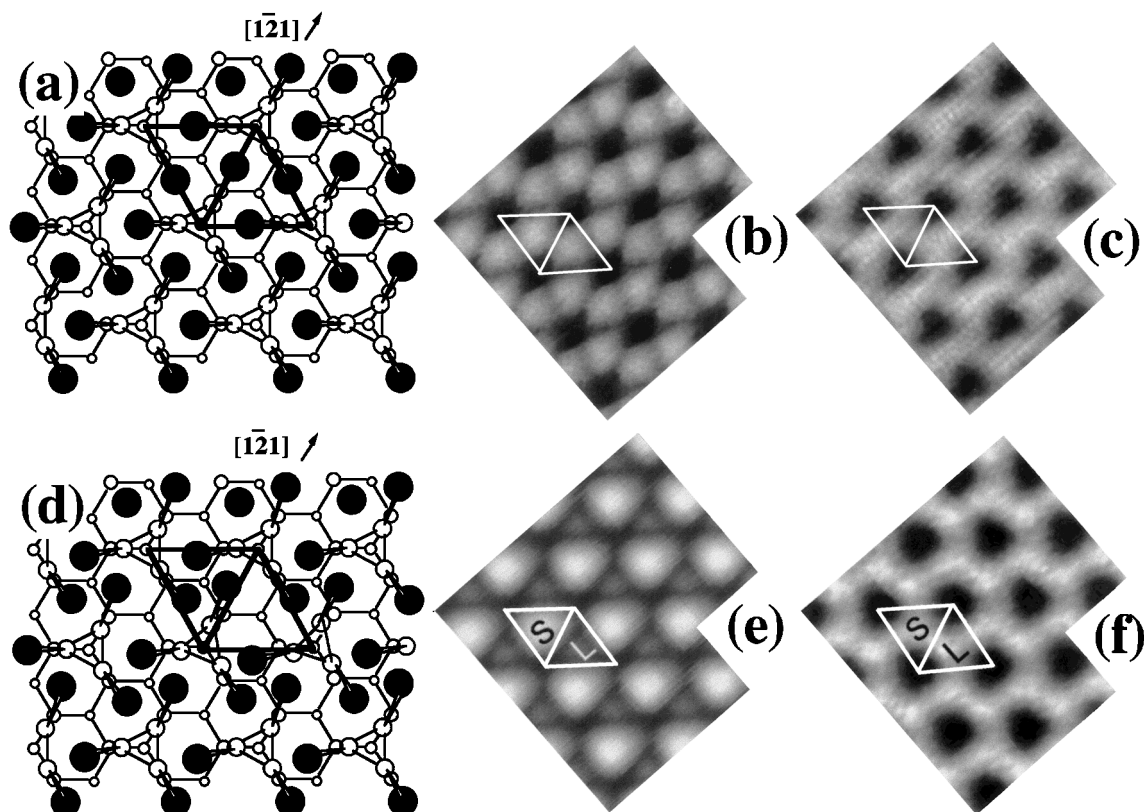


Fig. 2. Schematic illustrations and STM images of the Si(111)- $\sqrt{3} \times \sqrt{3}$ -Ag surface. (a) Its excited-state structure (so-called honeycomb-chained triangle (HCT) structure). Filled circles are Ag atoms, and open circles are Si atoms. A $\sqrt{3} \times \sqrt{3}$ -Ag unit cell is drawn. (b) Its empty-state and (c) filled-state STM images at RT. (d) Its ground-state structure (so-called inequivalent triangle (IET) structure). (e) Its empty-state and (f) filled-state STM images at 62 K.

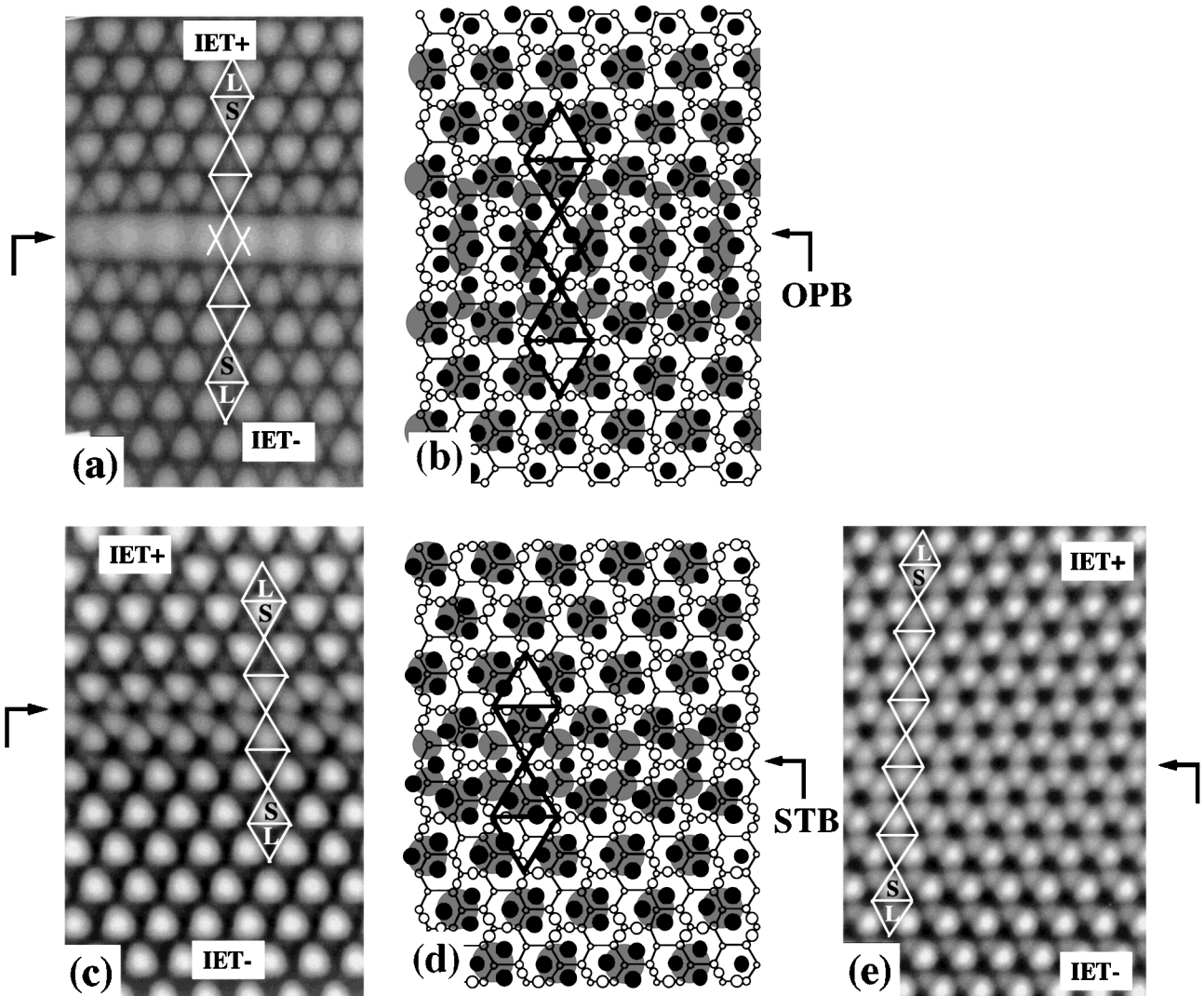


Fig. 3. STM images (a)(c)(e) and schematics (b)(d) of two types of domain boundaries on the Si(111)- $\sqrt{3} \times \sqrt{3}$ -Ag surface: (a)(b) out-of phase boundary (OPB), and (c)(d)(e) surface twin boundary (STB).

mains in twin relation, called IET+ and IET- domains, due to symmetry breakdown, between which surface twin boundaries (STBs) are created only at lower temperatures, as shown in Fig. 3(c). Such STBs are sometimes thin as shown in Fig. 3(d), or sometimes broad as shown in Fig. 3(e). Adjacent IET+ and IET- domains at a STB have no phase shift in the $\sqrt{3} \times \sqrt{3}$ -periodicity, but have opposite symmetry in the arrangement of L- and S-halves in the $\sqrt{3} \times \sqrt{3}$ unit cell (see Fig. 3(d)). The STBs are observed to fluctuate even at 6 K,⁴²⁾ indicating an easy conversion between IET+ and IET- domains, though the conventional OPBs never move even at RT. The STBs themselves indicate the validity of the asymmetric structure in the $\sqrt{3} \times \sqrt{3}$ unit cell.

3. Electronic Structure

Figure 4(a) shows a two-dimensional band dispersion diagram of the $\sqrt{3} \times \sqrt{3}$ -Ag surface, together with that of the 7×7 clean surface (Fig. 4(d)) for comparison, constructed from angle-resolved PES results.^{38,40)} The $\sqrt{3} \times \sqrt{3}$ -Ag surface is known to have three surface states, S1, S2, and S3 in (a); S1 is composed of a bonding state among Ag 5p orbitals at the Ag triangles. The S2 and S3 states stem mainly from Ag 5s orbital.⁴⁴⁾ Of these states, the S1 state has a

characteristic dispersion, i.e., a parabolic dispersion crossing E_F . Since its bottom is below E_F by about 0.2 eV, some electrons (1.6×10^{13} electrons/cm²) are accumulated in this surface-state band. This band is well reproduced by the first-principles calculation as shown in Fig. 4(c).³⁴⁾ Its large dispersion means an extended wavefunction of this state, having maximums in its local density of states at the centers of the Ag triangles,^{17,34)} corresponding to the protrusions in the empty-state STM images (Figs. 2(b) and 2(e)). This leads us to an expectation of a possible high electrical conductivity along the surface through this surface-state band.

Such a free-electron-like electronic state is visualized in low-temperature STM images in a form of the so-called *electron standing waves* or *Friedel oscillations*.⁴⁵⁾ Figure 5 shows an STM image of the $\sqrt{3} \times \sqrt{3}$ -Ag surface taken at 6 K (though the 7×7 clean domains partially remain, because of a Ag coverage smaller than 1 ML). In the $\sqrt{3} \times \sqrt{3}$ -Ag domains, fine periodic corrugations are seen, corresponding to the $\sqrt{3} \times \sqrt{3}$ -periodicity (as in Figs. 2(b) and 2(e)). Additionally, one can see standing wave patterns superimposed near step edges (A) and domain boundaries (B). In a small domain on the upper right, surrounded by steps and domain boundaries, a complicated concentric interference pattern is

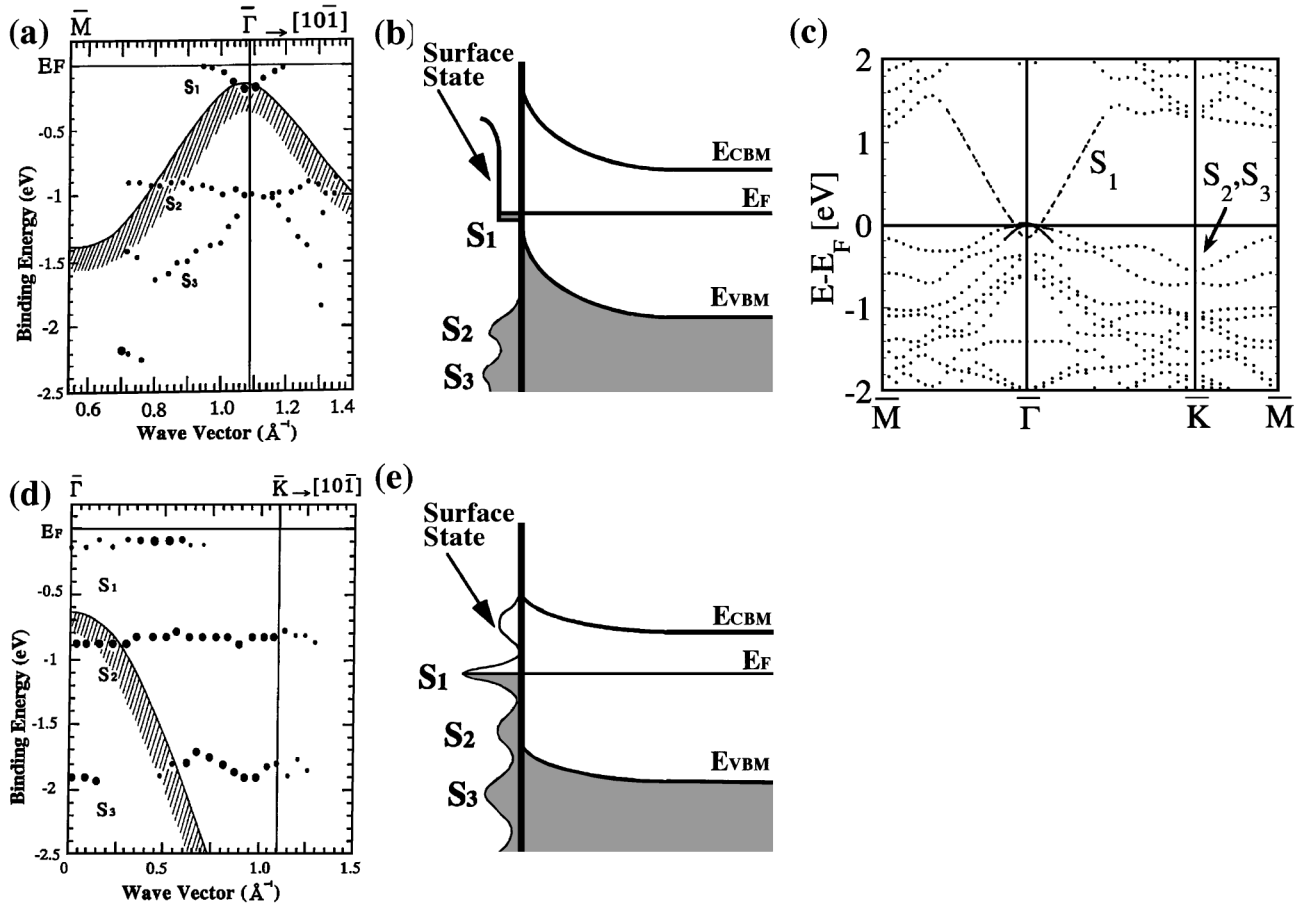


Fig. 4. Two-dimensional band dispersion diagrams of Si(111)- $\sqrt{3} \times \sqrt{3}$ -Ag (a)(c) and 7×7 clean (d) surfaces. (a) and (d) are constructed from angle-resolved PES measurements,³⁸⁻⁴⁰ while (c) is calculated by a first-principles theory.³⁴ (b) and (e) are schematic band diagrams showing band bending beneath the surfaces as well as the surface states of respective surfaces.

observed, while near the straight domain boundaries, the interference patterns are parallel to the OPB. Domain boundaries and atomic steps act as potential barriers for surface-state electrons, so that the reflected waves and incident waves interfere with each other to make the standing waves. By changing the bias voltage in STM imaging (in other words, by probing different energy levels), the wavelengths of the observed standing waves change according to a dispersion relation of the surface-state band.⁴⁵ This is an evidence for the wave patterns due to the electronic nature, rather than geometric undulation. In this way, the $\sqrt{3} \times \sqrt{3}$ -Ag surface is shown to have an extended surface electronic state.

The domain boundary (B) is an OPB as mentioned in §2.2, while the boundary (C) is a STB, at which no standing waves are observed. In other words, the STBs are transparent for the surface-state electrons. Then, an important and interesting question is raised here: what is the transmission coefficient of the electron wavefunction at step edges and domain boundaries? Although some studies assumed the step edge as a hard wall for surface-state electrons (that is, the transmission coefficient is zero),⁴⁶⁻⁵⁰ it should be questioned, because it governs an important parameter, i.e., the mobility of surface-state carriers. It is ascertained from Fig. 5 that the carrier mobility is lowered by carrier scattering by the step edges and domain boundaries. But how much lowered? The mobility of the surface-state electrons on the $\sqrt{3} \times \sqrt{3}$ -Ag surface is actually measured to be lower than that in bulk crystal by two orders of magnitude.⁵¹⁾

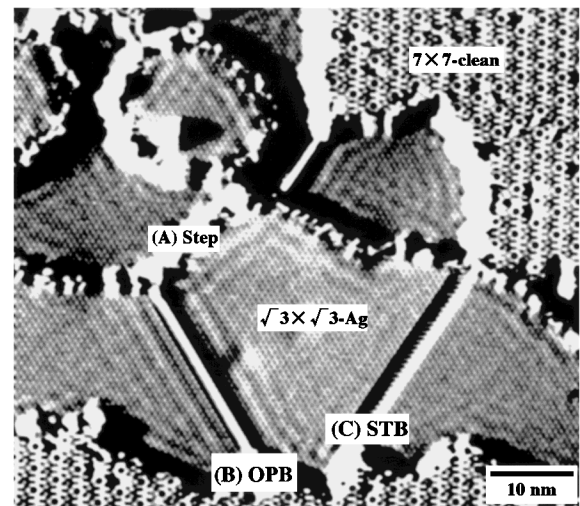


Fig. 5. Electron standing waves on the Si(111)- $\sqrt{3} \times \sqrt{3}$ -Ag surface, observed by STM at 6 K. The tunneling current is 0.5 nA with a sample bias of 0.75 V, probing empty states.⁴⁵⁾

In contrast, the 7×7 clean surface has an almost flat band near E_F , as shown in Fig. 4(d), which is known to come from the dangling-bond state on the topmost Si atoms. Its negligible dispersion indicates a localized nature, suggesting low conductivity along the surface through this surface state. This is indeed measured to be as low as on the order of 10^{-8} S/ \square .⁵²⁾

The surface-space-charge layers below the surfaces are also

in contrast between the 7×7 and $\sqrt{3} \times \sqrt{3}$ -Ag surface superstructures as shown in Figs. 4(b) and 4(e): a depletion layer below the 7×7 structure, while a hole-accumulation layer beneath the $\sqrt{3} \times \sqrt{3}$ -Ag structure. Therefore, electrical conductivity through the subsurface region is also expected to be different between these superstructures.

4. Electronic Transport

4.1 Carrier doping into the surface-state band

When two electric leads (*e.g.*, outer probes in linear four-point probe measurements, as illustrated in Fig. 6(a)) are connected to the surface of a semiconductor crystal with a macroscopic distance, and when a voltage is applied between them, the current flows through three channels on/in the crystal: (1) surface-state bands on the topmost atomic layers, (2) bulk-state bands in a surface-space-charge layer under the surface, and (2) huge bulk-state bands in the inner crystal. To measure the electrical conductivity through the surface-state band, one should carefully eliminate contributions from the underlying space-charge layer and bulk; quite a large fraction of the current tends to flow through the interior bulk in most cases.

In order to confirm the surface-state electrical conduction, conductivity measurements were done *in situ* in UHV by the four-point probe method with macroscopic probe spacings (approx. 10 mm), combined with electron diffraction to monitor surface structures, valence-band PES for analyzing surface electronic states, and core-level PES for measuring band bending beneath the surface to estimate conductivity through the surface-space-charge layer.¹⁾

One of the unambiguous ways to detect surface-state con-

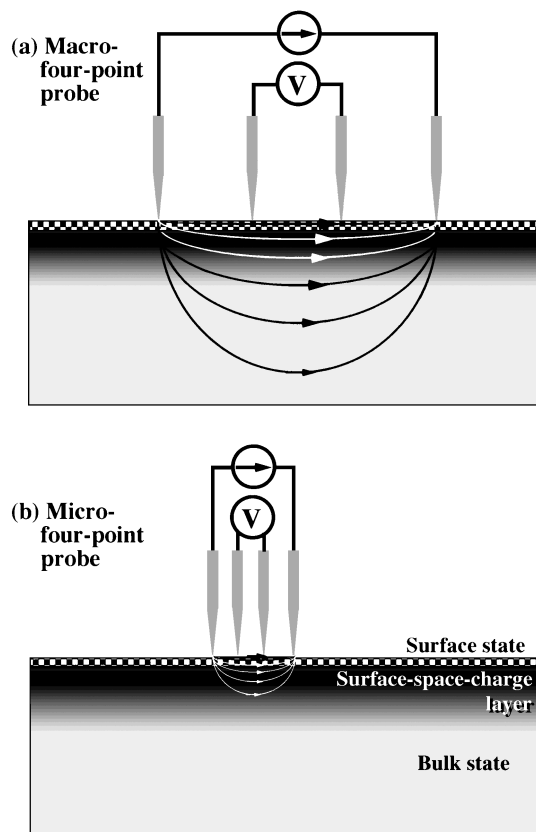


Fig. 6. Linear four-point probes in (a) macroscopic and (b) microscopic spacings, with schematic illustrations of current flow near a semiconductor surface.

ductivity is to measure a conductance change induced by a perturbation only to the surface region. Very small amounts (around 0.01 ML) of deposited atoms of monovalent metals (noble and alkali metals) on top of the $\sqrt{3} \times \sqrt{3}$ -Ag surface were found to adsorb in a form of monomers, an example of which is shown in Fig. 7,²⁴⁾ which is called '2D adatom-gas (2DAG) phase'.^{24,53)} Such 2DAG is found to enhance surface conductivity^{1,53)} due to electron doping into the surface-state bands. Figure 8(a) shows a resistance change during intermittent deposition of Ag atoms on top of the $\sqrt{3} \times \sqrt{3}$ -Ag surface at RT. Only 0.008 ML of Ag was deposited at each period of about 2 s, which caused a resistance drop as large as 10%. After interrupting the depositions by closing an evaporator shutter, the resistance remained constant during the intervals A, B, and C, which indicated that the observed resistance drops were due not to irradiation from the evaporator, but to the Ag adsorption. These changes in resistance were observed up to an additional Ag coverage of about 0.03 ML in total. Below this critical coverage, the adsorbed Ag atoms make the 2DAG phase, as shown in Fig. 7 (though the 2DAG cannot be directly observed by STM at RT, because of its very fast migration on the surface at RT). Beyond the critical coverage, the 2DAG begins to nucleate into three-dimensional Ag nuclei, which corresponds to the resistance recovery processes

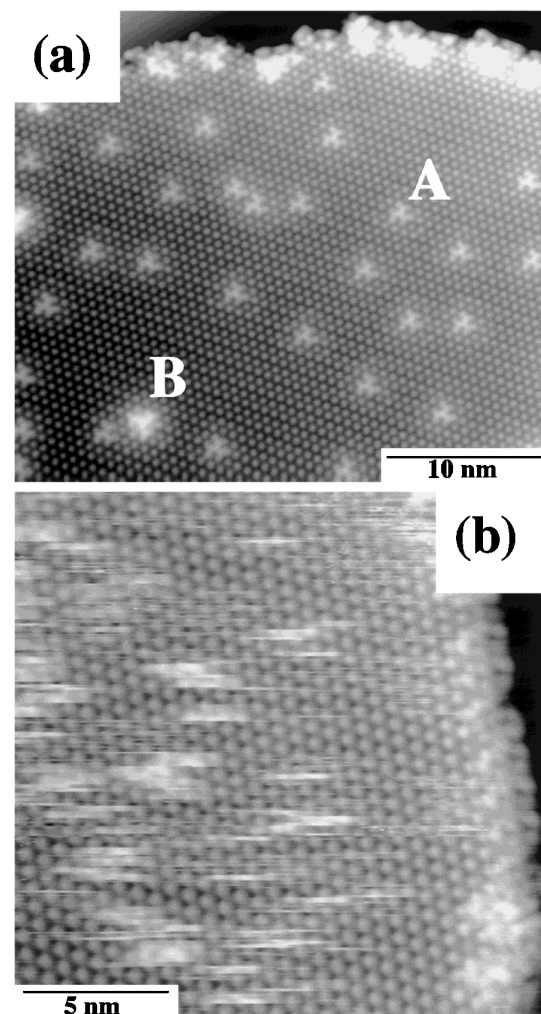


Fig. 7. Two-dimensional adatom gas (2DAG) of Ag on top of the Si(111)- $\sqrt{3} \times \sqrt{3}$ -Ag surface (a) frozen at 6 K, and (b) migrating at 65 K.²⁴⁾ Star-like protrusions indicated by A are single Ag adatoms, while clusters indicated by B are composed of three Ag adatoms.

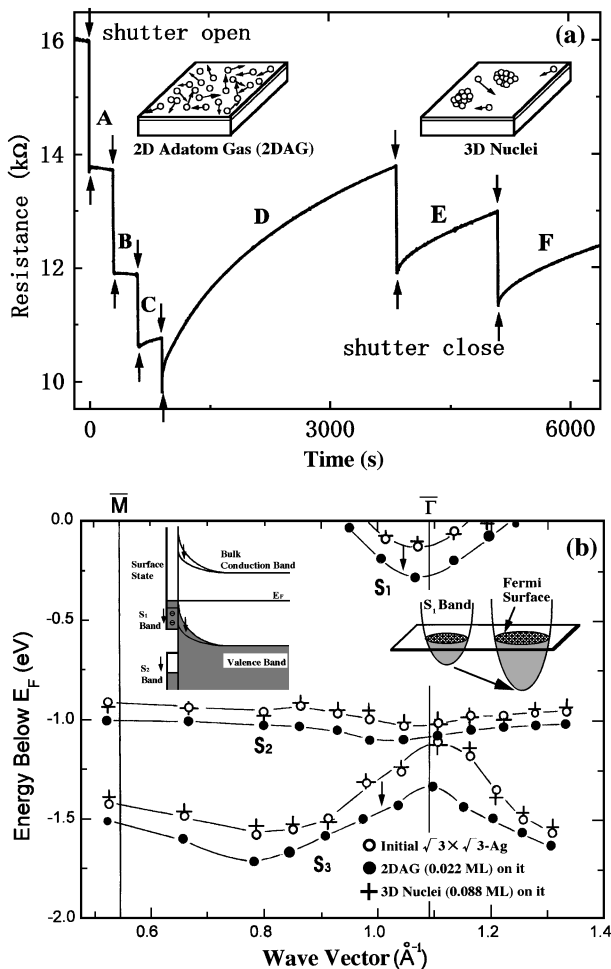


Fig. 8. Carrier doping into the surface-state band. (a) Resistance change of a Si(111) wafer with the $\sqrt{3} \times \sqrt{3}$ -Ag surface during intermittent deposition of Ag atoms at RT.⁵³⁾ The amount of each deposition for 2 s was about 0.008 ML, with intervals of 10–40 minutes. Downward arrows indicate the start of deposition, and upward arrows, the interruptions. A ~ F indicate the intervals. (b) Changes in the surface-state bands by Ag atom adsorption on the $\sqrt{3} \times \sqrt{3}$ -Ag surface, constructed from angle-resolved PES measurements. Open circles are for the initial $\sqrt{3} \times \sqrt{3}$ -Ag surface, solid ones, for the 2DAG-Ag (0.022 ML)-covered $\sqrt{3} \times \sqrt{3}$ -Ag surface, and crosses, for the 3D-Ag nuclei (0.088 ML)-covered one. Inset (left): Change in the surface-space-charge layer caused by the 2DAG adsorption.^{40,51)} Inset (right): 3D schematics of the S1 band with Fermi surfaces.

during intervals D, E, and F in Fig. 8(a).

From PES measurements of Si 2*p* core level in the bulk-sensitive mode, it turns out that the 2DAG makes the bulk bands beneath the surface flat as shown in the inset of Fig. 8(b). This means that the hole-accumulation layer under the initial $\sqrt{3} \times \sqrt{3}$ -Ag surface becomes a depletion layer, resulting in a decrease in conductivity through the surface-space-charge layer. Therefore, the observed resistance drop in Fig. 8(a) cannot be understood by the space-charge-layer conductivity.

From PES measurements of valence bands, it turns out that the 2DAG makes the surface-state bands shift downward, as shown in Fig. 8(b); the extent of shift is approximately equal to that for the above-mentioned Si 2*p* core-level shift. Due to this downward shift, the Fermi disk made of the S1 surface-state band grows, as shown in the inset of Fig. 8(b), indicating an increase in the number of electrons in this band, from $1.6 \times 10^{13} \text{ cm}^{-2}$ to $3.5 \times 10^{13} \text{ cm}^{-2}$. This leads to the increase in the number of conduction electrons, resulting in

the high conductivity. In this way, the electrical conduction through the surface-state band is confirmed experimentally.⁵¹⁾ The increase in the number of conduction electrons comes from the 2DAG, not from the bulk, because the bulk also accepts the electrons from the Ag adatoms to compensate the holes in the surface-space-charge layer. Therefore, it can be said that the adsorbed Ag atoms in the 2DAG phase donate their valence electrons to the surface-state band (and also to the space-charge layer) to increase conductivity. By comparing the number of deposited Ag adatoms and the increased numbers of electrons in the S1 band and the space-charge layer, each Ag adatom is found to provide approximately one electron to the substrate.^{1,39,51,53,54)}

There is another example to demonstrate surface-state conduction. By increasing the coverage of the 2DAG at RT, it begins to nucleate into 3D Ag nuclei, as mentioned above. But below 250 K, the 2DAG nucleates two dimensionally and arranges to make a new order, a $\sqrt{21} \times \sqrt{21}$ periodicity. The $\sqrt{21} \times \sqrt{21}$ superstructures are commonly formed by monovalent-atom adsorptions of about 0.15 ML on the $\sqrt{3} \times \sqrt{3}$ -Ag surface, and commonly have very high surface conductivities.^{1,29,30,54)} The reason for the high conductivity is again revealed by elaborate PES measurements that new dispersive metallic surface-state bands with large Fermi disks, inherent in the $\sqrt{21} \times \sqrt{21}$ superstructures, are created, while the surface-space-charge-layer conductance is suppressed. In this way, the surface-state electrical conduction is experimentally confirmed on Si(111)- $\sqrt{3} \times \sqrt{3}$ -Ag and $\sqrt{21} \times \sqrt{21}$ surfaces, whose sheet conductances are of the order of $10^{-4} \text{ S}/\square$, as measured by macroscopic four-point probes. This value is about four orders of magnitude higher than that for the dangling-bond surface state on the 7×7 clean surface.⁵²⁾

4.2 Micro-four-point probe

Micro-four-point probes with probe spacings down to $2 \mu\text{m}$ were developed at Mikroelektronik Centret of Technical University of Denmark (Fig. 9(a)).⁵⁵⁾ By reducing the dimensions of the probe spacing, as shown in Fig. 6(b), a larger fraction of current will flow near the surface, resulting in a more surface-sensitive measurement than by macroscopic four-point probes (Fig. 6(a)). Such probes were utilized in UHV to measure the surface-state conductivity of Si(111) surfaces, combined with a technique to control step configurations on the surface.⁵⁶⁾ By observing the probes and sample surfaces by *in situ* SEM, the probes were positioned on a large flat terrace, as shown in Fig. 9(b), where only a few atomic steps run between the inner probes, or on different terraces between which step bands are running as shown in Fig. 9(c). The resistance measured on a large terrace with almost step-free of the $\sqrt{3} \times \sqrt{3}$ -Ag surface (Fig. 9(b) on Fig. 1(e)) was smaller than that on a similar terrace of the 7×7 clean surface (Fig. 1(a)) by about two orders of magnitude. This was compared with measurements by macroscopic-four-point probes of about 10 mm probe spacing, where the difference in resistance between the two surfaces was as small as about 10%.⁵⁷⁾ These results mean that reducing the probe spacing makes the measurements more surface-sensitive, as expected in Fig. 6(b), and also because carrier scattering at step edges (as seen in Fig. 5) is suppressed by reducing the number of steps crossing the measured region. By adding Au adatoms of about 0.15 atomic layer on the $\sqrt{3} \times \sqrt{3}$ -Ag surface to make the $\sqrt{21} \times \sqrt{21}$ -

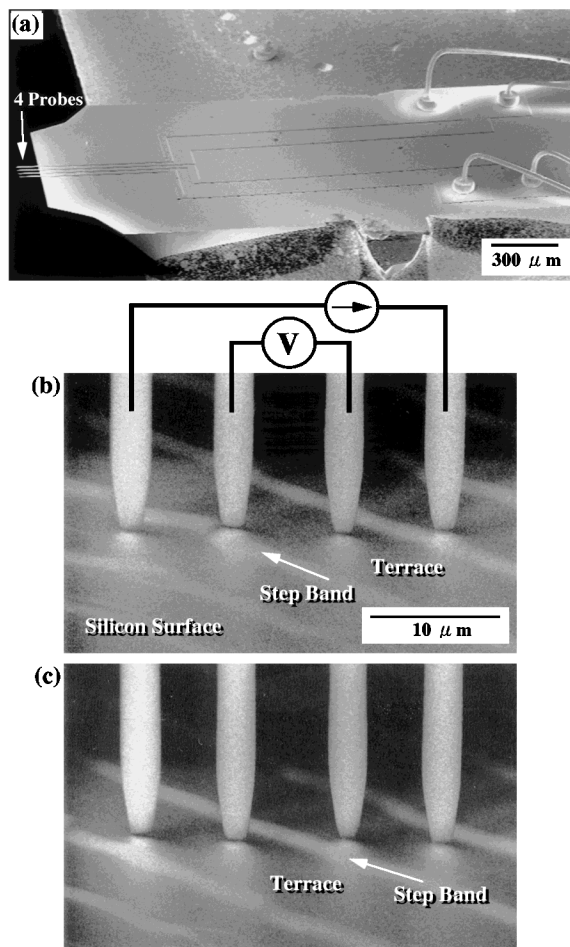


Fig. 9. Micro-four-point probe (μ -4PP). (a) A scanning electron micrograph of a μ -4PP chip. (b)(c) The μ -4PP contacting with the Si(111)- $\sqrt{3} \times \sqrt{3}$ -Ag surface in UHV-SEM. The inner probes are on a terrace in (b), while a step band is running between the inner probes in (c).

(Ag + Au) surface superstructure,^{25,26,29)} the resistance was further decreased by a factor of three. By converting the measured resistances into sheet conductances, we confirmed that the extremely high conductances of the $\sqrt{3} \times \sqrt{3}$ -Ag and $\sqrt{21} \times \sqrt{21}$ -(Ag + Au) surfaces are attributed to the surface-state bands inherent in the respective superstructures, rather than the conductivity of the surface space-charge layers. Although this conclusion was already reached by macroscopic-four-point probe measurements in UHV,^{1,29,38,39)} micro-four-point probe measurements made it much more convincing.

When a step band (where about 50 monatomic steps are accumulated) is running between the inner probes of the micro-four-point probes, as shown in Fig. 9(c), the measured resistances were much larger than those measured on a terrace with almost step-free on the same surface (Fig. 9(b)). This directly means that the step band region has a higher resistance than the terrace. This is because carriers in the surface-state bands are scattered by step edges, as seen in the form of electron standing waves in Fig. 5. These results will quantify the transmission coefficient of the carriers at individual step edges. Although such step-edge effect on surface electrical conductivity had been suggested in a point-contact measurement on the 7×7 surface,^{58,59)} our results confirmed it directly.

5. Conclusions

Direct experimental evidence of electrical conduction through the surface-state bands, inherent in surface superstructures, was obtained for the Si(111)- $\sqrt{3} \times \sqrt{3}$ -Ag surface and its relatives with the aid of highly sophisticated surface-science techniques such as STM and PES, and also a newly developed technique using micro-four-point probes. These studies will trigger more systematic investigations on the electronic transport properties of such an ultimate 2D-electron system, where the correlation with atomic arrangements on surfaces is essential. For example, *in situ* measurements of atomically controlled surfaces at low temperatures under a magnetic field in UHV are strongly desired. Furthermore, by utilizing technology for manipulating atomic-scale structures on surfaces, we should be able to control transport properties in novel ways. In addition to the expectations from the viewpoint of the fundamental physics of nanometer-scale systems, the transport properties of surface-state bands will be one of the most important subjects in nano-scale device performance.

Acknowledgments

This work was supported in part by Grants-in-Aid from the Ministry of Education, Science, Sports and Culture of Japan, especially through those for Creative Basic Research (No. 09NP1201) conducted by Professor K. Yagi of Tokyo Institute of Technology, and also for International Joint Research (No. 11694059). We were supported also by Core Research for Evolutional Science and Technology of the Japan Science and Technology Corporation, conducted by Professor M. Aono of Osaka University and RIKEN.

- 1) S. Hasegawa, X. Tong, S. Takeda, N. Sato and T. Nagao: *Prog. Surf. Sci.* **60** (1999) 89.
- 2) T. Takahashi, S. Nakatani, N. Okamoto, T. Ishikawa and S. Kikuta: *Jpn. J. Appl. Phys.* **27** (1988) L753.
- 3) T. Takahashi, S. Nakatani, N. Okamoto, T. Ishikawa and S. Kikuta: *Surf. Sci.* **242** (1991) 54.
- 4) T. Takahashi and S. Nakatani: *Surf. Sci.* **282** (1993) 17, and references therein.
- 5) M. Katayama, R. S. Williams, M. Kato, E. Nomura and M. Aono: *Phys. Rev. Lett.* **66** (1991) 2762.
- 6) G. LeLay, M. Gothelid, A. Cricenti, C. Hakansson and P. Perfetti: *Europhys. Lett.* **45** (1998) 65.
- 7) K. Yokoyama, T. Ochi, Y. Sugawara and S. Morita: *Phys. Rev. Lett.* **83** (1999) 5023.
- 8) N. Sasaki, H. Aizawa and M. Tsukada: to be published in *Appl. Surf. Sci.* (2000).
- 9) T. Yamaguchi: Meet. Abstr. the Physical Society of Japan, Vol. 54, Issue 1, Part 2, (Hiroshima Univ., March 1999) p. 301.
- 10) H. Hong, R. D. Aburano, D. S. Lin, H. Chen and T. C. Chiang: *Phys. Rev. Lett.* **68** (1992) 507.
- 11) H. Hong, R. D. Aburano, D. S. Lin, H. Chen and T. C. Chiang: *Phys. Rev.* **B52** (1995) 1839.
- 12) K. Akimoto, M. Lijadi, S. Ito and A. Ichimiya: *Surf. Rev. Lett.* **5** (1998) 719.
- 13) H. H. Weitering, J. P. Sullivan, R. J. Carolissen, W. R. Graham and R. T. Tung: *Surf. Sci.* **70/71** (1993) 422.
- 14) H. H. Weitering, J. P. Sullivan, R. J. Carolissen, W. R. Graham and R. T. Tung: *Appl. Surf. Sci.* **70/71** (1993) 422.
- 15) H. H. Weitering, J. P. Sullivan, R. J. Carolissen, W. R. Graham and R. T. Tung: *J. Appl. Phys.* **79** (1996) 7820.
- 16) T. Komizo, H. Hirayama and K. Takayanagi: Meet. Abstr. the Physical Society of Japan, Vol. 54, Issue 2, Part 4 (Iwate Univ., September 1999) p. 831.
- 17) S. Watanabe, M. Aono and M. Tsukada: *Phys. Rev.* **B44** (1991) 8330.

- 18) Y. G. Ding, C. T. Chan and K. M. Ho: Phys. Rev. Lett. **67** (1991) 1454.
- 19) Y. G. Ding, C. T. Chan and K. M. Ho: Phys. Rev. Lett. **69** (1992) 2452.
- 20) G. LeLay, M. Gotherlid, V. Yu Aristov, A. Cricenti, M. C. Hakansson, C. Giammichele, P. Perfetti, J. Avila and M. C. Asensio: Surf. Sci. **377-379** (1997) 1061.
- 21) T. Nakayama, J. Onoe, K. Takeuchi and M. Aono: Phys. Rev. **B59** (1999) 12627.
- 22) K. Tsuchie, T. Nagao and S. Hasegawa: Phys. Rev. **B60** (1999) 11131.
- 23) K. Iizumi, K. Ueno, K. Saiki and A. Koma: Meet. Abstr. the Physical Society of Japan, Vol. 54, Issue 2, Part 4 (Iwate Univ., September 1999) p. 815.
- 24) N. Sato, T. Nagao and S. Hasegawa: Phys. Rev. **B60** (1999) 16083.
- 25) A. Ichimiya, H. Nomura, Y. Horio, T. Sato, T. Sueyoshi and M. Iwatsuki: Surf. Rev. Lett. **1** (1994) 1.
- 26) J. Nogami, K. J. Wan and X. F. Lin: Surf. Sci. **306** (1994) 81.
- 27) I. Homma, Y. Tanishiro and K. Yagi: *The Structure of Surfaces 3*, eds. S. Y. Tong, M. A. Van Hove, K. Takayanagi and X. D. Xie (Springer, Berlin, 1991) p. 610.
- 28) Z. H. Zhang, S. Hasegawa and S. Ino: Phys. Rev. **B52** (1995) 10760.
- 29) C.-S. Jiang, X. Tong, S. Hasegawa and S. Ino: Surf. Sci. **376** (1997) 69.
- 30) X. Tong, S. Hasegawa and S. Ino: Phys. Rev. **B55** (1997) 1310.
- 31) X. Tong, Y. Sugiura, T. Nagao, T. Takami, S. Takeda, S. Ino and S. Hasegawa: Surf. Sci. **408** (1998) 146.
- 32) T. Nagao, S. Ohuchi, Y. Matsuoka and S. Hasegawa: Surf. Sci. **419** (1999) 134.
- 33) K. Oura, V. G. Lifshits, A. A. Saranin, A. V. Zotov and M. Katayama: Surf. Sci. Rep. **35** (1999) 1.
- 34) H. Aizawa, M. Tsukada, N. Sato and S. Hasegawa: Surf. Sci. **429** (1999) L509.
- 35) Y. Kondo, J. Nakamura and S. Watanabe: Abstr. Int. Symp. Surface Science for Micro- and Nano-Device Fabrication (Waseda Univ. Tokyo, Nov. 1999) p. 19.
- 36) L. S. O. Johansson, E. Landemark, C. J. Karlsson and R. I. G. Uhrberg: Phys. Rev. Lett. **63** (1989) 2092.
- 37) L. S. O. Johansson, E. Landemark, C. J. Karlsson and R. I. G. Uhrberg: Phys. Rev. Lett. **69** (1992) 2451.
- 38) S. Hasegawa, X. Tong, C.-S. Jiang, Y. Nakajima and T. Nagao: Surf. Sci. **386** (1997) 322.
- 39) S. Hasegawa, C.-S. Jiang, Y. Nakajima, T. Nagao and X. Tong: Surf. Rev. Lett. **3/4** (1998) 803.
- 40) X. Tong, C.-S. Jiang and S. Hasegawa: Phys. Rev. **B57** (1998) 9015.
- 41) A. Endo and S. Ino: Surf. Sci. **346** (1996) 40.
- 42) N. Sato, T. Nagao and S. Hasegawa: Surf. Sci. **442** (1999) 65.
- 43) T. Nakayama, S. Watanabe and M. Aono: Surf. Sci. **344** (1995) 143.
- 44) H. Aizawa and M. Tsukada: Phys. Rev. **B59** (1999) 10923.
- 45) N. Sato, S. Takeda, T. Nagao and S. Hasegawa: Phys. Rev. **B59** (1999) 2035.
- 46) T. Yokoyama, M. Okamoto and K. Takayanagi: Phys. Rev. Lett. **81** (1998) 3423.
- 47) T. Yokoyama and K. Takayanagi: Phys. Rev. **B59** (1999) 12232.
- 48) J. Li, W.-D. Schneider, R. Berndt and S. Crampin: Phys. Rev. Lett. **80** (1998) 3332.
- 49) Ph. Avouris, I.-W. Lyo, R. E. Walkup and Y. Hasegawa: J. Vac. Sci. Technol. **B12** (1994) 1447.
- 50) M. F. Crommie, C. P. Lutz, D. M. Eigler and E. J. Heller: Surf. Rev. Lett. **2** (1995) 127.
- 51) Y. Nakajima, S. Takeda, T. Nagao, S. Hasegawa and X. Tong: Phys. Rev. **B56** (1997) 6782.
- 52) S. Heike, S. Watanabe, Y. Wada and T. Hashizume: Phys. Rev. Lett. **81** (1998) 890.
- 53) Y. Nakajima, G. Uchida, T. Nagao and S. Hasegawa: Phys. Rev. **B54** (1996) 14134.
- 54) X. Tong, C.-S. Jiang, K. Horikoshi and S. Hasegawa: to be published in Surf. Sci. (2000).
- 55) P. Bøggild, C. L. Petersen, F. Grey, T. Hassenkam, T. Bjørnholm, I. Shiraki and S. Hasegawa: Proc. Transducers 99 (Sendai, Japan, June 1999).
- 56) T. Ogino: Surf. Sci. **386** (1997) 137.
- 57) C.-S. Jiang, S. Hasegawa and S. Ino: Phys. Rev. **B54** (1996) 10389.
- 58) Y. Hasegawa, I.-W. Lyo and Ph. Avouris: *Ultimate Limits of Fabrication and Measurement*, eds. M. E. Welland and J. K. Gimzewski (Kluwer, Dordrecht, 1995) p. 147.
- 59) Y. Hasegawa, I.-W. Lyo and Ph. Avouris: Surf. Sci. **358** (1996) 32.